MATHEMATICAL BIOSCIENCES
AND ENGINEERING
Volume **3**, Number **2**, Aprils **2006**

http://www.mbejournal.org/

pp. **419–440**

ANALYSIS OF BLOOD FLOW VELOCITY AND PRESSURE SIGNALS USING THE MULTIPULSE METHOD

Derek H. Justice

Department of Electrical Engineering and Computer Science
University of Michigan, Ann Arbor, MI 48109

H. Joel Trussell

Department of Electrical and Computer Engineering
North Carolina State University, Raleigh, NC 27695

Mette S. Olufsen

Department of Mathematics
North Carolina State University, Raleigh, NC 27695

(Communicated by James F. Selgrade)

Abstract. This paper shows how the multipulse method from digital signal processing can be used to accurately synthesize signals obtained from blood pressure and blood flow velocity sensors during posture change from sitting to standing. The multipulse method can be used to analyze signals that are composed of pulses of varying amplitudes. One of the advantages of the multipulse method is that it is able to produce an accurate and efficient representation of the signals at high resolution. The signals are represented as a set of input impulses passed through an autoregressive (AR) filter. The parameters that define the AR filter can be used to distinguish different conditions. In addition, the AR coefficients can be transformed to tube radii associated with digital wave guides, as well as pole-zero representation. Analysis of the dynamics of the model parameters have potential to provide better insight and understanding of the underlying physiological control mechanisms. For example, our data indicate that the tube radii may be related to the diameter of the blood vessels.

1. **Introduction.** During posture change from sitting to standing, blood is pooled in the lower extremities as a result of increased gravitational potential. A response to the shift in blood volume from the thorax to the lower extremities is a decrease in venous return, cardiac filling pressure, and cardiac output. The decreased cardiac output causes a decrease in arterial blood pressure, which in turn may cause a decrease in cerebral blood flow. To restore arterial blood pressure and maintain cerebral blood flow, two main control mechanisms are activated. Autonomic regulation, mediated by the central nervous system as a response to changes in aortic and carotid blood pressure, causes an increase in heart rate, cardiac contractility, peripheral resistance, compliance, and unstressed volumes of blood vessels in

2000 *Mathematics Subject Classification.* 92D30.

Key words and phrases. blood flow and pressure dynamics, signal processing, multipulse method, mathematical modeling.

the thorax and lower extremities. Simultaneously, cerebral autoregulation (a local control that responds to changes in myogenic activity and the concentration of carbon-dioxide) maintains cerebral blood flow by decreasing the cerebral vascular resistance. In healthy young people, cardiovascular regulation maintains a constant blood flow despite changes in blood pressure. In healthy elderly people, the regulation is still viable, but may be diminished. Even for hypertensive individuals, it is assumed that regulation is maintained, but it is shifted to be active at higher pressures [1]. For people with diminished regulation, the cardiac output may not be fully restored after posture change from sitting to standing, hence the blood flow to the brain may be reduced, which can cause transient "black outs" or dizziness.

To study the regulation mechanism, simultaneous recording of blood pressure and blood flow velocity have been recorded during posture change from sitting to standing. In this paper, we show that the multipulse method from digital signal processing (DSP) can be used to analyze the two signals independently. The parameters that define the multipulse method form an "input" signal that consists of a few impulses and a set of autoregressive (AR) coefficients. Previously, this method of generating an AR representation without specific knowledge of the input has proved to be useful in speech signal processing [2, 3, 4, 5] as well as in geophysical applications [6]. We show how the method can be used to analyze blood pressure and blood flow velocity signals obtained during posture change from sitting to standing. The parameters obtained from the method show definite differences between three groups of subjects: 1) healthy young subjects, 2) healthy elderly subjects, and 3) hypertensive elderly subjects.

Blood pressure from these subjects is recorded in the middle finger of the non-dominant hand and the blood flow velocity is recorded in the left middle cerebral artery (MCA). These signals are chosen because reliable measurements from these vessels are easy to obtain non-invasively [1, 7, 8, 9]. The advantage of including signals from two distinct locations in the brain and in the body is that we are able to investigate how cerebral autoregulation interacts with autonomic regulation that mainly acts in the torso and lower extremities. Ideally, one would prefer to analyze both blood pressure and blood flow velocity signals from each location, but it is not possible to obtain non-invasive measurements of blood pressure in the brain. One could possibly include blood pressures measured in the ear-lobe, but it needs to be investigated if the vessels in the ear-lobe are big enough to provide accurate and reliable blood pressure recordings. Blood flow velocity can be measured in the upper body, for example, in the radial artery (the arteries in the finger are too small to obtain reliable blood flow velocity recordings). For the current study, we are limited to the two signals measured in the brain and in the finger, but in future work, we plan to include additional velocity recordings from the radial artery.

Most previous studies characterize the effect of either cerebral autoregulation [10]-[21] regulating vascular resistance, or baroreflex function (an autonomic regulation) [22]-[30], regulating the heart rate and vascular resistance. Most analysis methods, including our method, predicting cardiovascular regulation are based on a linear representation of the system [15]. A popular method to predict the effect of autoregulation is based on a linear transfer function where blood pressure is treated as an input and blood flow velocity is the output (for example, see [1, 7, 10, 11, 12, 14, 15, 16, 17, 19, 21]). Conclusions about autoregulation are obtained by using the transfer function between the blood pressure signal and the blood flow velocity signal to compute the coherence between the two signals. These

works infer that a high coherence between blood pressure and blood flow velocity indicates that the blood flow velocity follows the blood pressure, while a low coherence (the range of autoregulation) appearing shortly after posture change indicates that blood flow velocity is regulated differently than the blood pressure. Another approach for addressing the effect of autoregulation and autonomic function has been to characterize the cardiovascular system by a linear analog circuit with two resistors representing the systemic and peripheral resistance and a capacitor representing the compliance of the MCA [20] (the three element windkessel model [31]). This method also uses a transfer function to represent the relation between the two signals. The effect of the cardiovascular regulation is obtained by studying the variation in the parameters, i.e., the two resistors and the capacitor. The times at which the peripheral resistance is decreased are interpreted as the region of autoregulation [20, 32]. A new approach suggested by Panerai et al. uses a neural network model to analyze the dynamics of cerebral autoregulation [33]. This work used a time-lagged recurrent neural network model to analyze the dynamic relationship between arterial blood pressure and cerebral blood flow velocity. The model was compared with standard models and provided an output that was not significantly different from results obtained from time-domain techniques.

The baroreflex function has been addressed by closed-loop models that predict the regulation by describing effects of the entire cardiovascular system [22]-[28]. With these models, it is difficult to analyze the signals because complex methods are needed to estimate parameter values and changes in parameter values. One attempt to combine a closed-loop model with data analysis is the model by Olufsen, et al. [34], which is based on optimal control strategies. Similar models are presented in the work [35, 36, 37]. Finally, the multiscale model proposed by Fernandez, Millisic, and Quaterioni [38] could be used to study regulation of blood flow.

Except for the closed-loop models, all the approaches discussed above are presumptuous about the input, namely, that pressure causes flow. As we show in this paper, it is possible that a separate signal originating from the brain or the heart, such as the electrocardiogram (EKG), could act as the input or contribute to the input for both pressure and flow. One previous paper attempted to relate changes in pressure to changes in heart rate in order to study the regulation process during progressive lower-body negative pressure. This method describes the baroreflex function using an autoregressive-moving average (ARMA) approach [28]. It used a 4 Hz sampling rate and a second-order AR representation with a pure 0.75 sec delay of the input pressure signal. This was adequate for quantities that are averaged over the time of a heartbeat. Our method is able to use a higher sampling rate to represent the signals accurately between heartbeats with a model of the signal whose parameters model the system over the time of several heartbeats.

In addition, most previous contributions base their analysis on mean values of the blood pressure and blood flow velocity. Effects such as the widening of the blood flow velocity (increase in difference between the systolic value and the diastolic value) can not be captured by such models. Previous analysis [1, 7, 20] has shown that this widening may be significantly different for young individuals and for elderly or hypertensive elderly. Hence, we find it important to develop analysis methods that take these aspects into account. Our method computes a sequence of the input pulses while at the same time deriving an AR representation. This allows us to represent the signal at high resolution between heartbeats. However, the value of DSP approach is not the approximation of the signal but the modeling of the

system that creates the signal. This is done over the time interval of several cardiac cycles. The system parameters that characterize the vascular system are sampled on the order of the speed of the control mechanisms, which have been estimated at about 0.3 Hz. Thus, the AR representation describes the signal characteristics over a time interval that is large with respect to the sampling interval. The representation of the signal is done efficiently by using only a few parameters. Some of the parametric forms that we develop are very likely to relate to physical quantities of interest. The fact that the signal can be reproduced very well lends credibility to the characterization based on this parametric mathematical model. Furthermore, the AR representation permits diverse interpretation by the examination of other derived system parameters, such as reflection coefficients, tube radii, poles and zeros. Finally, the digital description can be transformed into an analog model using common DSP methods. This allows the extension of our method to analog models such as those discussed in [20, 25, 27, 36, 39]. The multipulse DSP method is extremely versatile. It is hoped that it will lead to improved interpretation of vascular control mechanisms.

2. **Methods.**

2.1. **Experimental Setup.** For this study, data were collected from 29 subjects with two recordings for each subject. The subjects include 9 healthy young subjects, 10 healthy elderly subjects, and 10 hypertensive elderly subjects. All subjects were pre-screened for known diseases and to ensure that adequate signals could be obtained. Beat-to-beat arterial blood pressure was determined non-invasively from the middle finger of the non-dominant hand, using a photoplethysmographic non-invasive pressure monitor (Finapres), supported by a sling at the level of the right atrium to eliminate hydrostatic pressure effects. Blood flow velocity in the left MCA was measured using trans-cranial Doppler (TCD) ultrasound. A 2 MHz probe of a Nicolet Companion portable Doppler system was strapped over the temporal bone and locked in position with a Mueller-Moll probe fixation device to image the MCA. The MCA blood flow velocity was identified according to the criteria of Aaslid [40] and recorded at a depth of 50–65 mm. The envelope of the blood flow velocity waveform, derived from a Fast-Fourier analysis of the Doppler frequency signal, and continuous pressure signals were digitized at 500 Hz and stored in the computer for later off-line analysis.

Following instrumentation, subjects sat in a straight-backed chair with their legs elevated at 90 degrees in front of them on a stool. For each of two active stands, subjects rested in the sitting position for 5 minutes, then stood upright for one minute. The initiation of standing was timed from the moment both feet touched the floor. Data were collected continuously during the final minute of sitting and the first minute of standing during both trials [20]. A diagram of the experimental setup is shown in Figure 1.

The data used for this study have been published earlier, and are used with permission from Dr. Lipsitz's laboratory [1]. The study was approved by the Institutional Review Board at the Hebrew Senior Life, and all subjects provided written informed consent.

Representative blood pressure and blood flow velocity signals are shown in Figure 2. Signals from three individuals are shown: a healthy young subject, a healthy elderly subject, and a hypertensive elderly subject. These signals are representative with other subjects within each population. The higher blood pressure is apparent

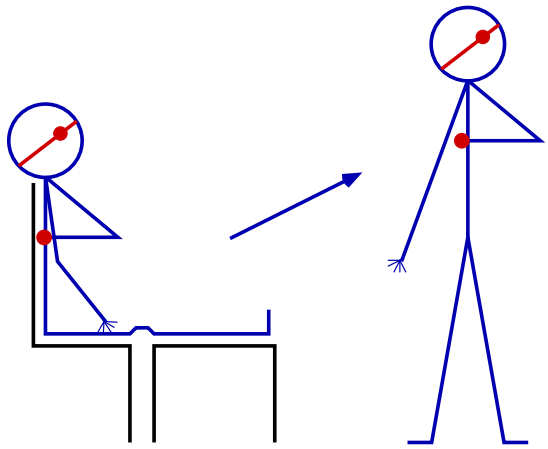

FIGURE 1. Experimental setup. Initially, the subject was seated for approximately one minute, then told to stand. The blood pressure is measured non-invasively from them middle finger of the non-dominant hand, using a photoplethysmographic non-invasive pressure monitor (Finapres), supported by a sling at the level of the right atrium to eliminate hydrostatic pressure effects. The blood flow velocity is measured using the 2 MHz probe of a Nicolet Companion portable Doppler system strapped over the temporal bone.

in the hypertensive subject. During posture change (at 60 sec), one can note the drop in arterial blood pressure in the finger. This is due to the effect of gravity pooling the blood into the lower extremities, which leads to a reduction in venous return followed by a decrease in cardiac output. The decreased cardiac output leads to a drop in arterial blood pressure in the upper body and an increase in blood pressure and blood flow to the lower extremities. Another consequence of the decreased arterial blood pressure is a potential reduction of mean blood flow velocity to the brain. In response to the reduction of systemic blood pressure autonomic control mechanisms are activated, and as a result the blood pressure is restored to normal approximately 20 sec after the posture change. Furthermore, cerebral autoregulation is activated to maintain constant cerebral blood flow velocity.

2.2. **Multipulse Representation.** Since the blood pressure and blood flow velocity signals are recorded in digital format, it is natural to consider representing the signals using common DSP methods. The signals in Figure 2 show several properties that are common in voiced speech signals, for example, an almost periodic form and a natural decay after an initial peak. The multipulse method introduced in [2] and currently found in most modern texts on speech signal processing (for example, see [5]) can be easily modified for use in this case. The modification of the method that is used in this work is discussed in [3].

The basic premise of the multipulse method is that the signal (either the blood pressure or the blood flow velocity), $y(n)$, can be represented using the standard autoregressive method (AR),

$$y(n) = \sum_{k=1}^{P} \alpha(k) y(n-k) + x(n), \tag{1}$$

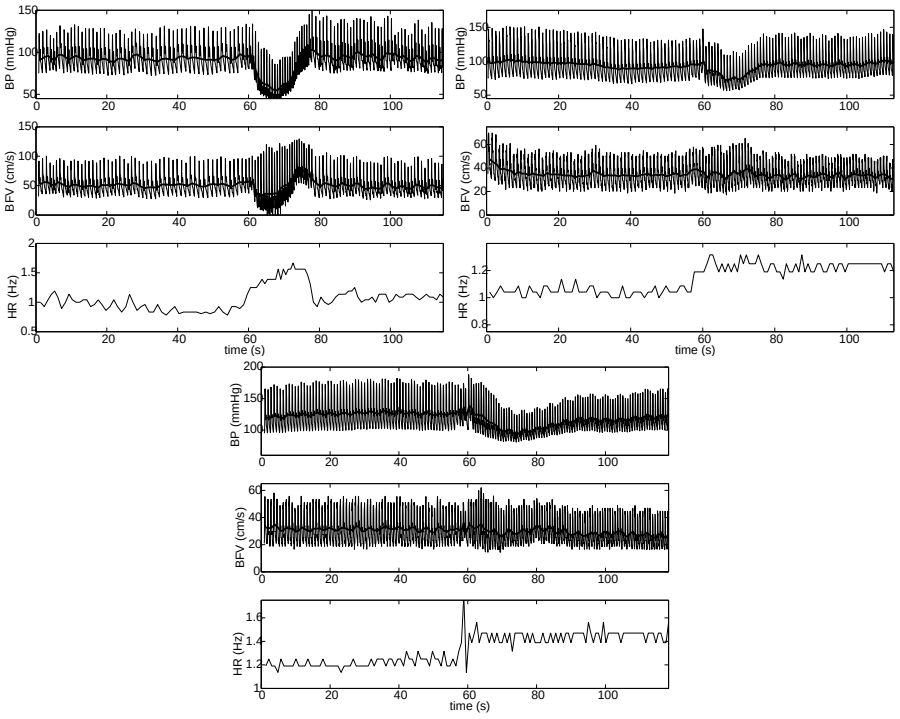

FIGURE 2. Example blood pressure (BP), blood flow velocity (BFV), and heart rate (HR) for a young subject (left), a healthy elderly subject (right), and a hypertensive elderly subject (bottom). The blood pressure and blood flow velocity are plotted along with their mean values (solid line through the oscillating signals). Note that the drop in blood pressure and blood flow velocity (especially for the young subject) corresponds to an increase in heart rate, this is part of the regulation mechanism.

where P is the order of the method, $\alpha(k)$ is the k^{th} AR coefficient, and $x(n)$ is the input. For this system, the input could be thought of as the EKG. However, since the two signals are analyzed separately, an input for each signal will be determined, and these inputs will not be the same. In a real physiological system, one common input (for example, EKG) would create both outputs, but the two outputs may depend on the input differently. How these two inputs may be related will be studied in future work. The *multipulse* innovation is that the input to the AR system is a series of discrete impulses $\delta(n - p_i)$ at times p_i with amplitudes $b(i)$. Mathematically, this is given by

$$x(n) = \sum_{i=1}^{I} b_i \delta(n - p_i). \tag{2}$$

In speech applications, the impulses are related to high and low air pressure pulses generated by the vocal chords. For this work, the pulses could be related to contraction and relaxation of the heart, a relationship that could be studied by measuring additional quantities, such as simultaneous recording of the EKG. Such work is

proposed but is beyond the scope of the current paper. The goal is to solve simultaneously for the AR coefficients $\alpha(k)$, the pulse positions $\Omega_{pp} = \{p_1,\ p_2, \ldots, p_I\}$, and amplitudes $\{b_1, b_2, \ldots, b_I\}$ that minimize the squared error

$$\sum_n \left(y(n) - \left(\sum_{k=1}^{P} \alpha(k) y(n-k) + x(n) \right) \right)^2, \tag{3}$$

where $y(n)$ is the recorded blood pressure or blood flow velocity signal. This leads to a non-linear system of equations that is difficult to solve. Iterative schemes have been found to produce acceptable solutions. These schemes are based on a procedure that uses current estimates of the impulses to obtain new AR coefficients; and then uses the new AR coefficients to compute a new set of impulses. A given iteration begins with estimates of the set of impulses, Ω_{pp}. The AR coefficients are estimated using the data at all times at which an impulse does not appear, given the current estimate of the impulses. The mathematical form of the minimization problem that is used to estimate the AR coefficients is a linear system given by

$$\alpha = arg \left(\begin{array}{c} min \\ \alpha \end{array} \left[\sum_{n \notin \Omega_{pp}} \left(y(n) - \sum_{k=1}^{P} \alpha(k) y(n-k) \right)^2 \right] \right). \tag{4}$$

We use the AR coefficients, $\alpha(k)$, to solve for the unknown impulses. The output estimate is computed using

$$\hat{y}(n) = \sum_{k=1}^{P} \alpha(k) y(n-k). \tag{5}$$

The location of the I largest errors in magnitude of the set of errors $\{e(n) = \hat{y}(n) - y(n)\}$ is used to define the position of the impulses and the negative of the errors are used to define the amplitude of the impulses. The iteration is started with Ω_{pp} taken as the empty set. The iteration is terminated when the positions of the impulses do not change in successive iterations.

An important difference between speach signals and blood pressure/flow signals is the difference in the mean values of the signals. Speech signals have values that vary about a mean of zero. Blood pressure and blood flow velocity signals vary above a baseline pressure or velocity. The natural decay of the AR system when no pulses are present produces the asymptotic value of zero. This presents no problem for speech signals. However, it is necessary to modify blood pressure and blood flow signals to allow the AR method to be effective.

Since the AR method produces a signal that naturally decays to zero when no input is present, it is natural to remove the baseline values. To do so, we fitted a low-order polynomial to the minimum values of the signals over the region of interest. Our method, subtracts this minimum function to produce a secondary signal that is suitable for application of the multipulse method. This minimum function is added back in to complete the reconstruction of the signals after the multipulse parameters are found and the output according to equation (1) is computed.

The physical interpretation of the parameters obtained from applying the multipulse method is subjective. Following the analogy of the interpretation of speech modeling, the AR coefficients represent a characterization of the vascular system and the impulses represent a characterization of the input, which may be thought of as the heartbeat or the EKG signals that control the heartbeat. The interpretation

of the minimum function that is removed prior to applying the multipulse method might be related to some control mechanism, but this is still under investigation.

2.3. **Representation and Fitting.** Blood pressure and blood flow velocity signals were recorded from subjects who fall into one of three categories: healthy young subjects aged 21-28 years, with an average blood pressure of 93 mmHg, healthy elderly subjects aged 64-86 years, with an average blood pressure of 87 mmHg, and hypertensive elderly subjects aged 67-86 years, with an average blood pressure of 114 mmHg. Two separate recordings were performed for each subject, and there were 9 healthy young subjects, 10 healthy elderly subjects, and 10 hypertensive elderly subjects.

Because the signals were oversampled at 500 Hz, decimation was feasible without fear of losing characteristic parts of the spectra. Furthermore, in order to use the multipulse method, the pulses that appear in the sampled signal must be narrow enough to be adequately represented by the signal impulse. To accomplish this, the signal was downsampled to 25 Hz.

Any DSP method will use only a finite amount of data. The trade-off is between using enough samples to get accurate estimates of the parameters by averaging out the noise, and using few enough samples to track time-varying phenomena. For this work, we used overlapping segments of four cardiac cycles. A single cycle is about one second. The averaging process will smooth the variations and each averaged value then represents about 4 sec, or a response rate of 0.25 Hz. This is about the response time of the control mechanism [1]. A cardiac cycle may be defined as the time from one landmark in the cycle to the next occurrence of the same mark, for example, the time of maximum pressure or velocity. For our work, we identified the minimum value that occurred immediately before a maximum value. A series of such cycle boundaries is shown in Figure 3. The process is as follows: the parameters that characterize the signal model are estimated for a number of samples that make up four cardiac cycles, then there is a shift of one cycle and the parameters of the signal for the next four cycles are estimated. For example, estimation of the parameters of the signal is carried out for cycles {1,2,3,4}, then {2,3,4,5}, then {3,4,5,6}, etc.

The pressure pulse-wave is ejected from the heart and propagates towards the periphery with a certain wave propagation speed. The wave propagation speed depends on the physical properties of the blood and vascular system, as well as the mean pressure[1]. Since the two signals (blood pressure and blood flow velocity) are measured at different locations, a delay is introduced that depends on the difference between the distance from the heart and the MCA and from the heart to the finger, as shown in Figure 1. This delay had to be addressed in order to determine the correspondence between the timing of the blood pressure and the blood flow velocity signals. It was accounted for by determining starting and stopping points for the blood pressure signal and simply shifting them to obtain the corresponding points in the blood flow velocity signal.

For each set of four cycles, a fourth-order AR representation ($P = 4$) was computed with 32 pulses ($I = 32$) after detrending the minimum of equation (1). The fourth-order representation was chosen to represent a low-order model that would be consistent with other work in this area. Previous work with analog models used

[1]The speed would vary with the pressure during systole and diastole. We assume that this variation in speed would result in insignificant variations in our parameters.

either first- or second-order differential equations (for example, see [20]). We first tried second-order digital models but found them to give poor signal representations, particularly for the healthy and hypertensive elderly subjects. Hence, we investigated higher-order models. This investigation showed that for models of order higher than four, the high-order terms all approached zero. The fourth-order system can represent a fourth-order differential equation or two coupled second-order differential equations.

In order to generate a reconstructed signal, the pulses for each set were filtered with the AR coefficients, and the detrending polynomial was added back. This computation is shown below.

$$\begin{aligned} y_{ar}(n) &= \sum_{k=1}^{P} \alpha(k) y_{ar}(n-k) + x(n) \\ \hat{y}(n) &= y_{ar}(n) + d(n), \end{aligned} \tag{6}$$

where $\hat{y}(n)$ is the reconstructed signal, $x(n)$ is the computed pulse train shown in equation (2), and $d(n)$ is the second-order detrending polynomial.

For tabulation and analysis, the results associated with each cycle were the average of the results for each of the four overlapping data sets. For example, the average AR coefficients for cycle 4 are computed by equally weighting the AR coefficients from sets {1,2,3,4}, {2,3,4,5}, {3,4,5,6}, and {4,5,6,7}. The input pulses and signal reconstruction over the cycle are averaged in the same way. Let us consider an example of this averaging as shown in Figure 4. The 72^{nd} cycle is defined by the time limits of 61.53 and 62.16. This region is marked by vertical lines in each of the top four graphs. The four graphs show the successive four cycles of the computation that include the 72^{nd} cycle, (i.e., {69,70,71,72}, {70,71,72,73}, {71,72,73,74}, {72,73,74,75}). The four pulse sequences associated with the 72^{nd} cycle are averaged to form the pulse average shown in the bottom graph of the figure. In this case, all of the estimated pulse sequences appear quite consistent for the four estimations. Minor variations can be seen in some of the other cycles. The fact that the plots of input pulses sometimes appear as continuous waveforms results from impulses occurring adjacent to each other.

3. **Analysis.**

3.1. **Signal Reconstruction.**

Fifty-eight total data sets were processed with two trials for each of 9 healthy young subjects, 10 healthy elderly subjects, 10 hypertensive elderly subjects. Sample errors of the blood pressure and blood flow velocity signals from their reconstructions, $\epsilon(n) = \hat{y}(n) - y(n)$, are shown in Figure 5 along with the computed input pulses superimposed on the detrending polynomial (i.e., $x(n) + d(n)$). The reconstructions are plotted with the original signal and input pulses on a smaller scale in Figure 3.

Note that the reconstructed signal matches the original signal quite well. The error signal-to-noise ratio (SNR) is given by $\mathrm{SNR}_{dB} = 20 \log\left(\sigma_{y(n)}/\sigma_{\epsilon(n)}\right)$. The fact that these are quite large (around 20 dB) indicates that our method reconstructed the signals well. The flow error SNR's are lower in almost all cases due to the noise present in the flow signals. Averages and standard deviations of the error SNR's for each group are listed in Table 1. The good SNR ratios indicate that the signals can be synthesized well using the parameters obtained from our analysis. This indicates

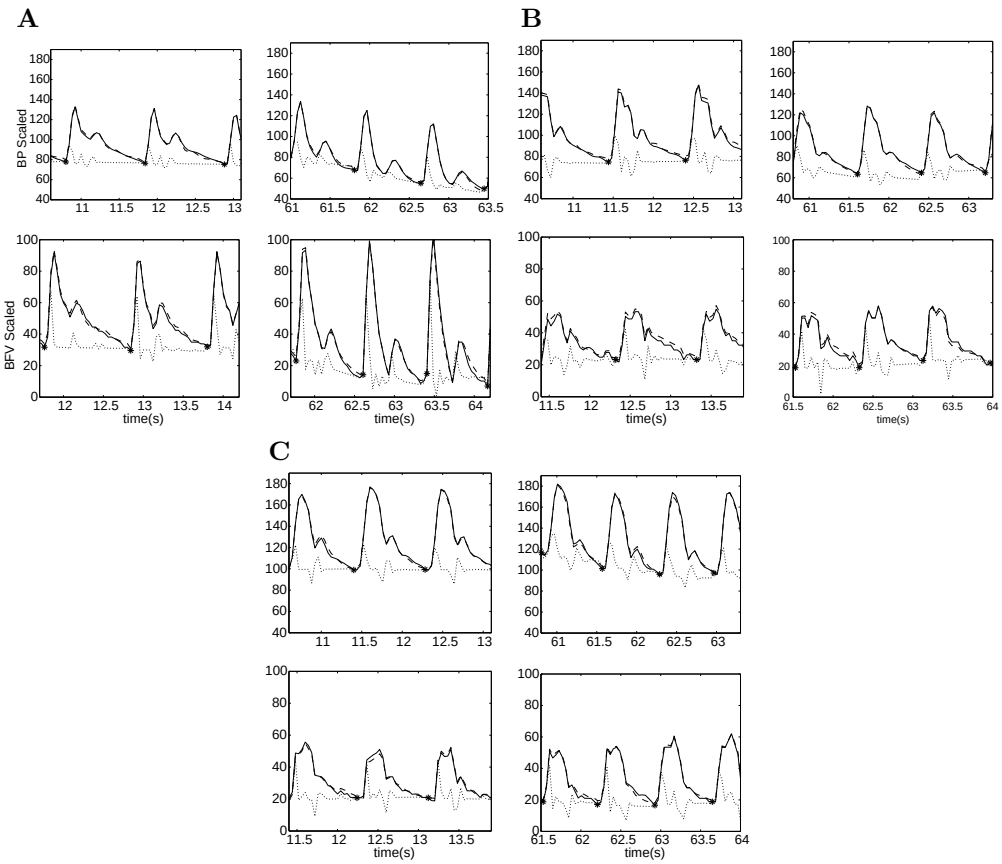

FIGURE 3. Scaled view (2.5 sec shown) of blood pressure (BP) top graphs and blood flow velocity (BFV) bottom graphs (solid lines), along with the Reconstruction (dashed lines), input pulses (dotted lines), and cycle boundaries (asterisks). Results from a healthy young subject are shown in A; those from a healthy elderly subject are shown in B; and those from the hypertensive elderly subject are shown in C.

that the parameters are consistent and can be used to accurately characterize the signal.

One of the most significant advantages of the multipulse method is that it allows inclusion of variable pulse positions. This enables analysis of irregular heartbeats and signal anomalies without distorting the AR representation of the vascular system. Note the irregularity of the hypertensive subject's heartbeat in Figure 2 around 60 sec. As is shown in Figure 5, there is no significant effect on the error signal at this time. This will be important later when we show the various output parameters as a function of time. We will see a smooth transition in those values around such irregularities.

3.2. **Time-Domain Representations: AR Coefficients, Reflection Coefficients, Tube Radii.** The AR coefficients are the straightforward representation

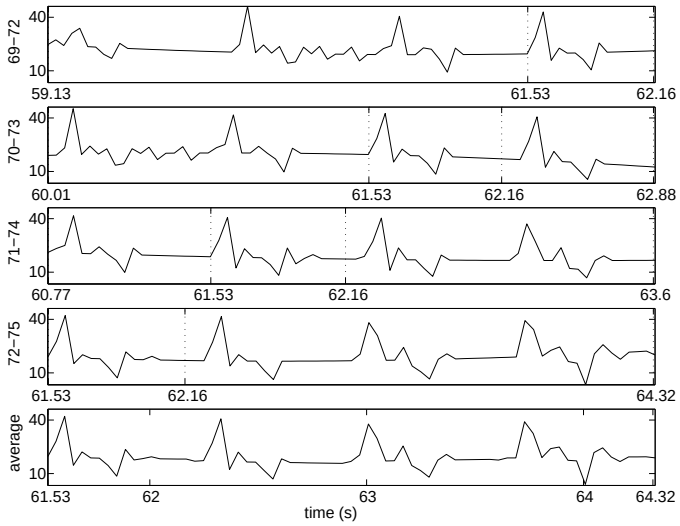

FIGURE 4. Demonstration of input pulse averaging for a single period of the blood flow velocity signal. The input pulses for period 72 are delineated between grid lines in the graphs. As shown, these segments are averaged from models computed for cycles 69-72, 70-73, 71-74, and 72-75 to generate the corresponding time segment of averaged input pulses for cycles 72-75 in the bottom plot.

Error signal-to-noise ratios (dB).

Signal Type	Young	Healthy Elderly	Hypertensive Elderly
Pressure	23.17 ($\pm$3.104)	22.96 ($\pm$1.082)	24.08 ($\pm$1.786)
Flow Velocity	18.94 ($\pm$3.083)	16.88 ($\pm$1.777)	16.85 ($\pm$1.719)

TABLE 1. The error signal-to-noise ratios are computed as $\mathrm{SNR}_{dB} = 20\log\left(\sigma_{y(n)}/(\sigma_{\hat{y}(n)-y(n)})\right)$, where $y(n)$ is the original blood pressure or blood flow velocity signal, $\hat{y}(n)$ is the corresponding reconstructed signal, and $\sigma_{f(n)}$ is the standard deviation for a signal $f(n)$. Results are given in the form average ($\pm$ standard deviation) where these statistics are computed for all subjects within the specified category.

of the parameters in equation (1). However, there are other parameterizations of the AR system that may be of interest. The digital waveguide form is of particular interest, since it uses the physical model of an acoustic tube to describe the system. In the waveguide representation, the system is considered to be a tube that consists of a sequence of equal-length segments of varying radii. The number of segments corresponds to the order of the AR system. The length of each segment is determined by the speed of sound in the medium, in this case blood, and the sampling rate of the digital system. The length corresponds to the distance required for sound to travel the length of the tube in one sampling interval. The change in

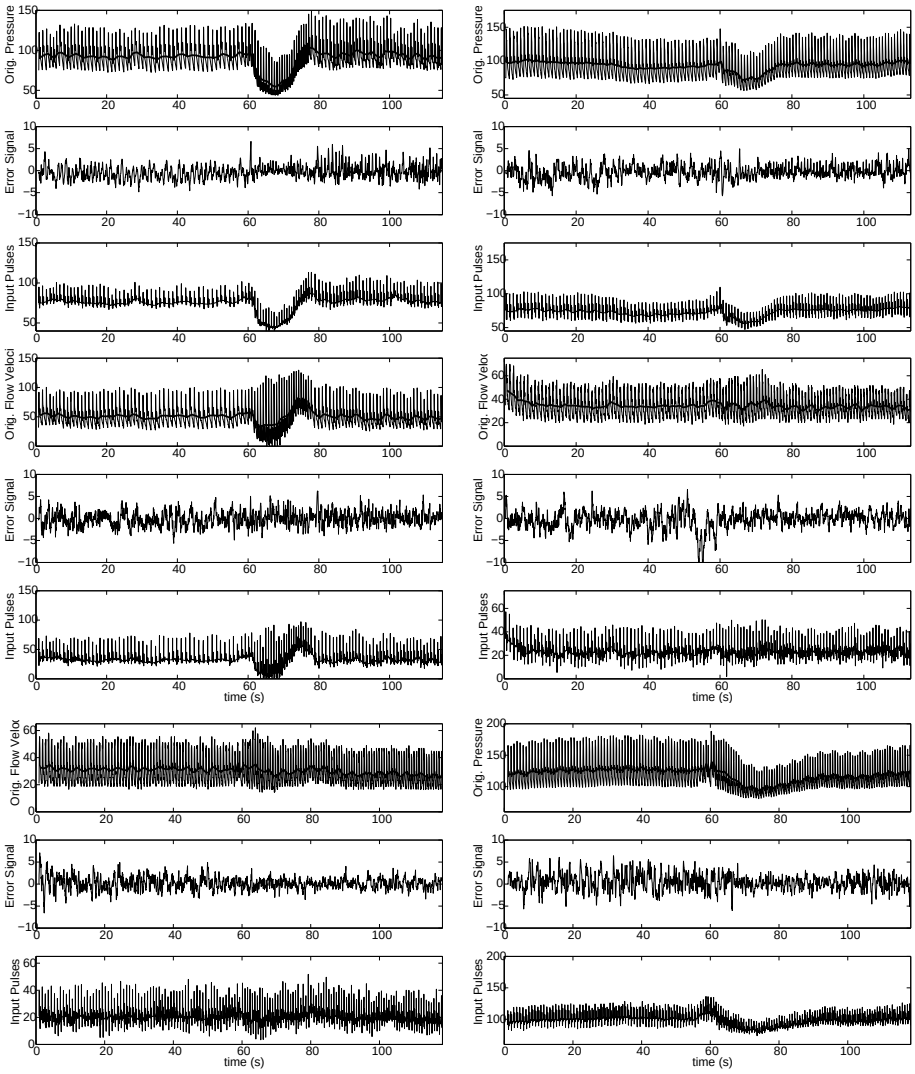

FIGURE 5. Example signals with error signals and input pulses. The error signal is defined as the difference between the original signal and its reconstruction. The input pulses are superimposed on the detrending polynomial. Analysis of blood pressure signals (top three panels) for a healthy young subject (left), a healthy elderly subject (right), and a hypertensive elderly subject (bottom). Corresponding analysis of the blood flow velocity signals are shown in the bottom three panels. Solid lines through the pressure and velocity signals and the input pulses indicate mean values.

radii results in the division of the input energy into reflected and transmitted components. To find the tube radii, we first compute the reflection coefficients $\{K_i\}$ from the AR coefficients. Reflection coefficients are used in lattice implementations of digital filters. They may be computed directly from the AR coefficients via the

Schur-Cohn equations that are found in any digital systems text. The relation between the reflection coefficients and the tube radii $\{R_i\}$ is associated with the interface between the i^{th} and $(i+1)^{th}$ segments

$$K_i = \frac{R_i - R_{i+1}}{R_i + R_{i+1}}. \tag{7}$$

The details can be found in readily available DSP texts, such as [41, 42].

The system characterizations (AR coefficients and tube radii) are plotted in Figure 6 for the blood pressure signals and in Figure 7 for the blood flow velocity signals. Since we used a fourth-order method, there are five AR coefficients. The zeroth-order coefficient is normalized to unity. Similarly, the radius of the first tube was taken as one, and the rest were computed recursively from the reflection coefficients using the relation in equation (7). In Figures 6 and 7, each asterisk represents the corresponding AR coefficient for an individual cycle, computed as described in the previous section.

The tube radii parameters have the potential to yield results that relate to physical quantities. The graphs indicate that the parameter tends to behave in a more stable way than the AR coefficients. They are also more stable than the reflection coefficients that are not shown to save space. The tube radii associated with the blood pressure increase immediately after standing and returns to normal after 20 sec of standing for the healthy young and the healthy elderly subjects. However, corresponding parameters associated with the blood flow velocity maintain almost constant values. A detailed interpretation of these results is beyond the scope of this paper, which introduces the multipulse method for analyzing the signals. However, it is intriguing to see the difference in the behavior of the three parameters. A brief discussion of possible physiological implications of these parameter variations is given in the discussion.

As noted previously, the multipulse method can account for irregular heartbeats and signal anomalies. As seen in Figure 6, all of the output parameters have a smooth transition through the region of the irregular heartbeat in the blood pressure signal about time $t = 60$ sec. This is the result of the ability to place a pulse at the correct time of the actual flow anomaly.

3.3. **Frequency Domain Representation: System Poles.** An alternative frequency domain representation of the AR method can be developed by taking the z-transform of equation (1). One can consider system poles, which give insight into the dynamic behavior of the signal. The transfer function can be represented in the z-domain as

$$H(z) = \frac{Y(z)}{X(z)} = \sum_{k=1}^{P} \frac{r_k}{1 - p_k z^{-1}}, \tag{8}$$

where r_k is the k^{th} residue and p_k is the k^{th} pole. $Y(z)$ represents the output of the system (blood pressure or blood flow velocity), while $X(z)$ is the input. The fourth-order method ($P = 4$ in equation (8)) gives four poles that must be real or they must occur in conjugate pairs. Only a few of the data analyzed in this paper gave four real poles. The most prevalent combination was two real poles and one conjugate pair.

The phase of a complex pole gives the frequency of oscillation in the time-domain associated with that pole, while the magnitude gives the degree of damping

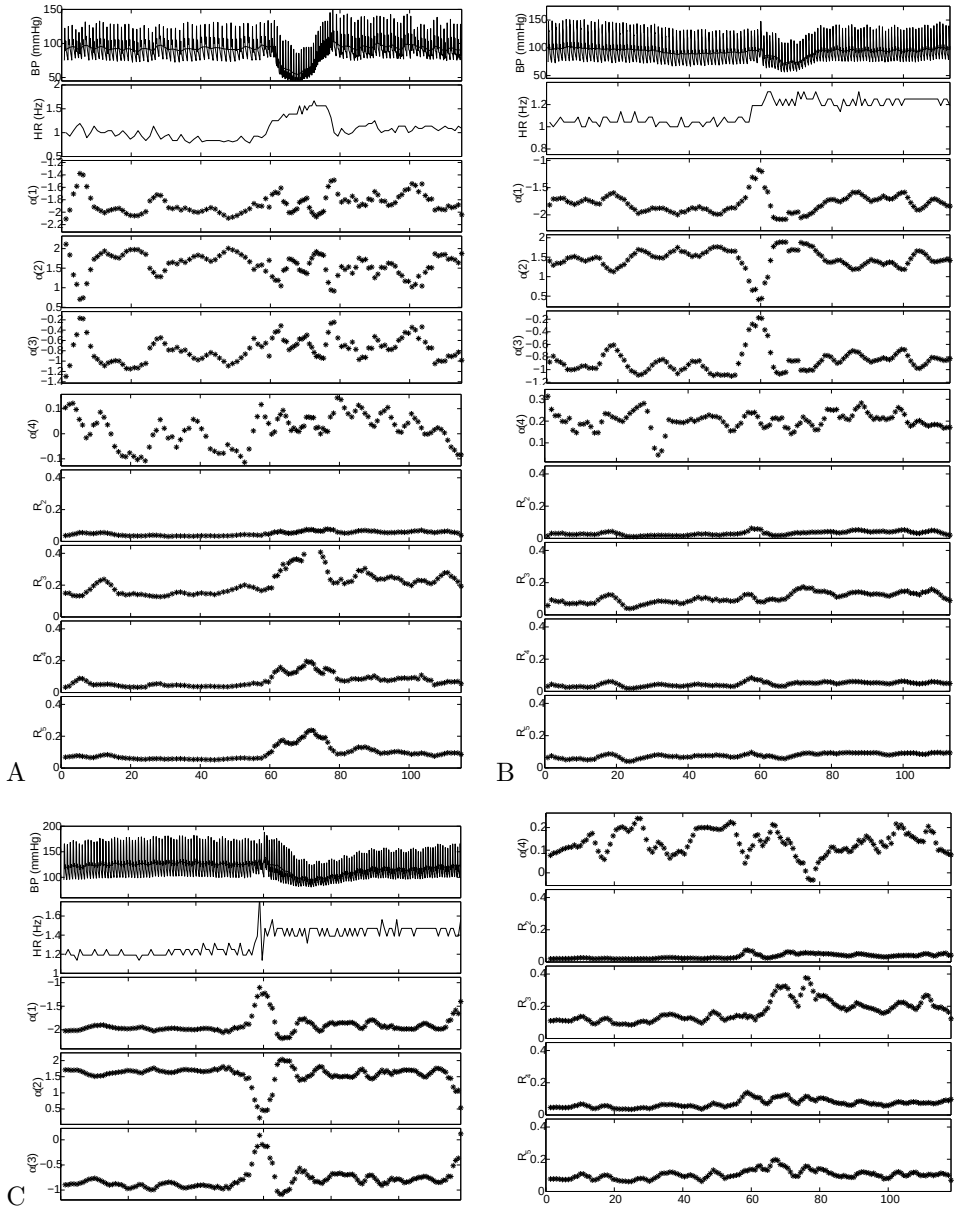

FIGURE 6. Time variation of output parameters obtained when predicting the blood pressure (BP) signal for a healthy young subject (A), a healthy elderly subject (B), and a hypertensive elderly subject (C). The original blood pressure signal is shown along with the heart rate (HR) for comparison. Each star in the plot represents the computed parameters averaged for a single cycle. The different representations are shown: AR coefficients ($\alpha(1) - \alpha(4)$) and tube radii($R_2 - R_5$, R_1 is normalized to unity).

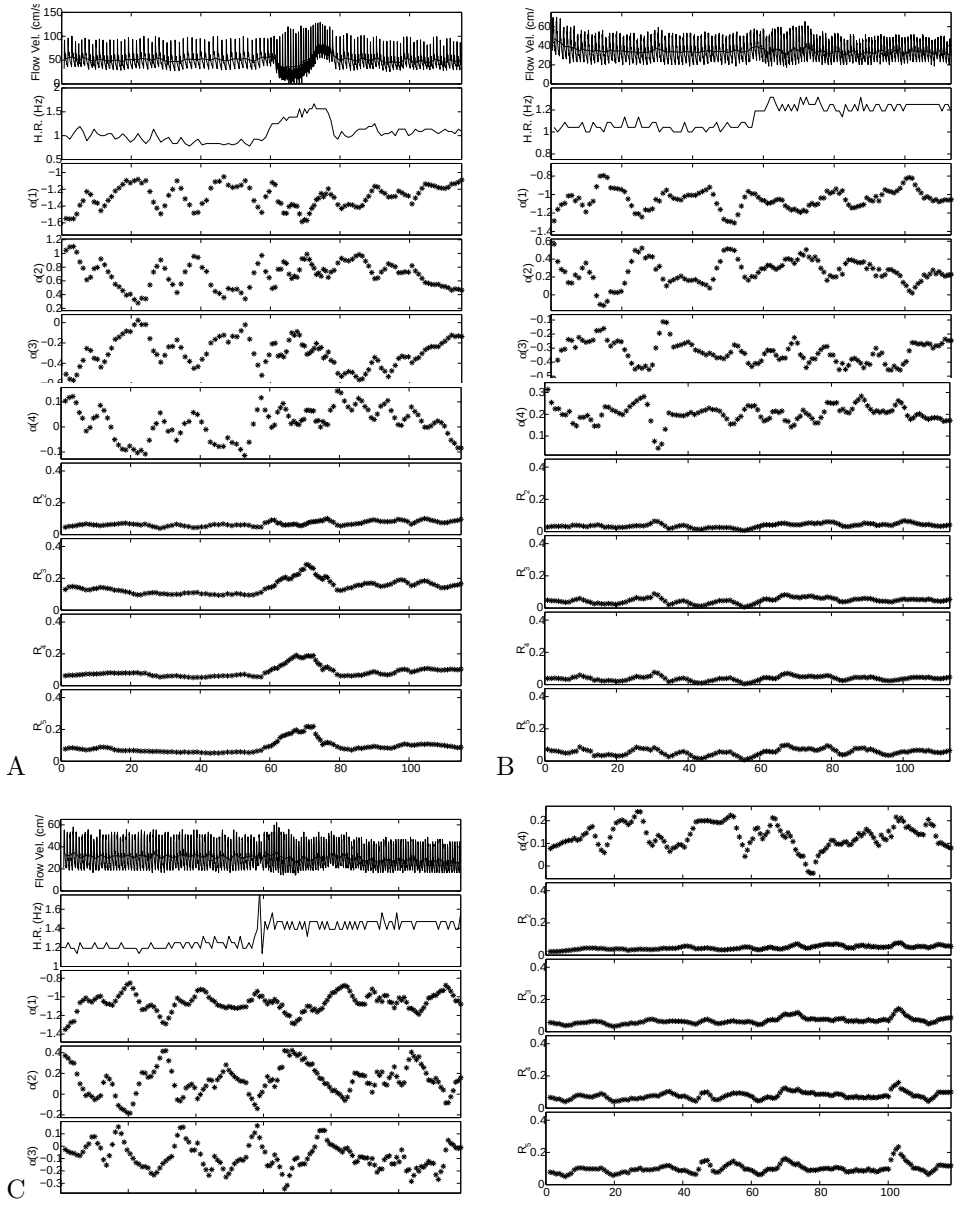

FIGURE 7. Time variation of output parameters obtained when predicting the blood flow velocity (BFV) signal for a healthy young subject (A), a healthy elderly subject (B), and a hypertensive elderly subject (C). The original blood flow velocity signal is shown along with the heart rate (HR) for comparison. Each star in the plot represents the computed parameters averaged for a single cycle. The different representations are shown: AR coefficients ($\alpha(1) - \alpha(4)$) and tube radii($R_2 - R_5$, R_1 is normalized to unity).

(see [42]). Most of the data sets have a high-frequency pole, $\omega_h > 3$ Hz. A low-frequency pole, $\omega_l < 3$ Hz, appeared more often in the data sets for the healthy elderly subjects. In the sets for healthy young subjects, it was commonly the case that two real poles were obtained instead of a lower-frequency complex pair. Plots of the pole variation for sample blood pressure and blood flow velocity signals are shown in Figures 8 and 9. These plots show both the distribution of poles within the unit circle and the behavior of the poles as a function of time. As in the case of the three time-domain parameters, the pole behavior is closely correlated with the transition to standing.

At present, no physical interpretation is associated with the pole movement. However, there do appear to be noticeable differences between the three classes of subjects. The reader is reminded that the frequency associated with the poles is not related to the frequency of the heartbeat, but is related to the physical characterization of the vascular system.

4. **Summary and Extension.** The autoregressive method can successfully reproduce the blood pressure and blood flow velocity signals to a high degree of accuracy (see the error SNRs in Table3.1). The different time and frequency domain representations presented have potential to provide insight into the regulation mechanisms at work.

Referring to Figure 6, one can discern a change in the AR coefficients needed to represent the blood pressure signals during the transition region (60-80 sec), especially, for the healthy and hypertensive elderly subjects, while there is no noticeable difference in the AR coefficients needed to represent the blood flow velocity signals (see Figure 7). The tube radii parameters show a different aspect of transition region. The tube radii show distinct increase during the transition for the healthy young subject, little for the healthy elderly subject, and only a slight change for the hypertensive elderly subject. For the blood flow velocity signals (see Figure 7), only the healthy young subject shows a distinct change. This might be due to the effect of autoregulation, which maintains blood flow velocity under a changing blood pressure. For both signals, our analysis shows a significant difference between the healthy young subject and the two elderly subjects. For the healthy young subject, especially the tube radii vary significantly more than for the elderly subjects. This may be explained from the fact that elderly people and especially people with hypertension have stiffer arteries that do not change as much. Furthermore, for the elderly subjects the heart-rate changes more (it increases and stays increased). This indicates that the regulation mainly affects the heart-rate, while the resistances are affected to a lesser degree. The subjects displayed in the figures are representative for the three groups, but a more detailed analysis is needed to tease out quantitative differences between the groups.

The plots of the system poles shown in Figures 8 and 9 also vary significantly between the three groups. A significant variation in the high-frequency pressure pole ω_h is noted in Figure 8, especially over the transition region (60-80 sec). There is a change in both magnitude and frequency of ω_h; however, the magnitude drop appears to lead the frequency drop. Again, note that the behavior of the blood flow velocity signal (see Figure 9) does not appear to follow the pressure signal. In addition, a noticeable difference in the blood flow velocity signal is observed between the healthy young subject and the two elderly subjects. For the healthy young subject, we see a significant change in both magnitude and phase, whereas

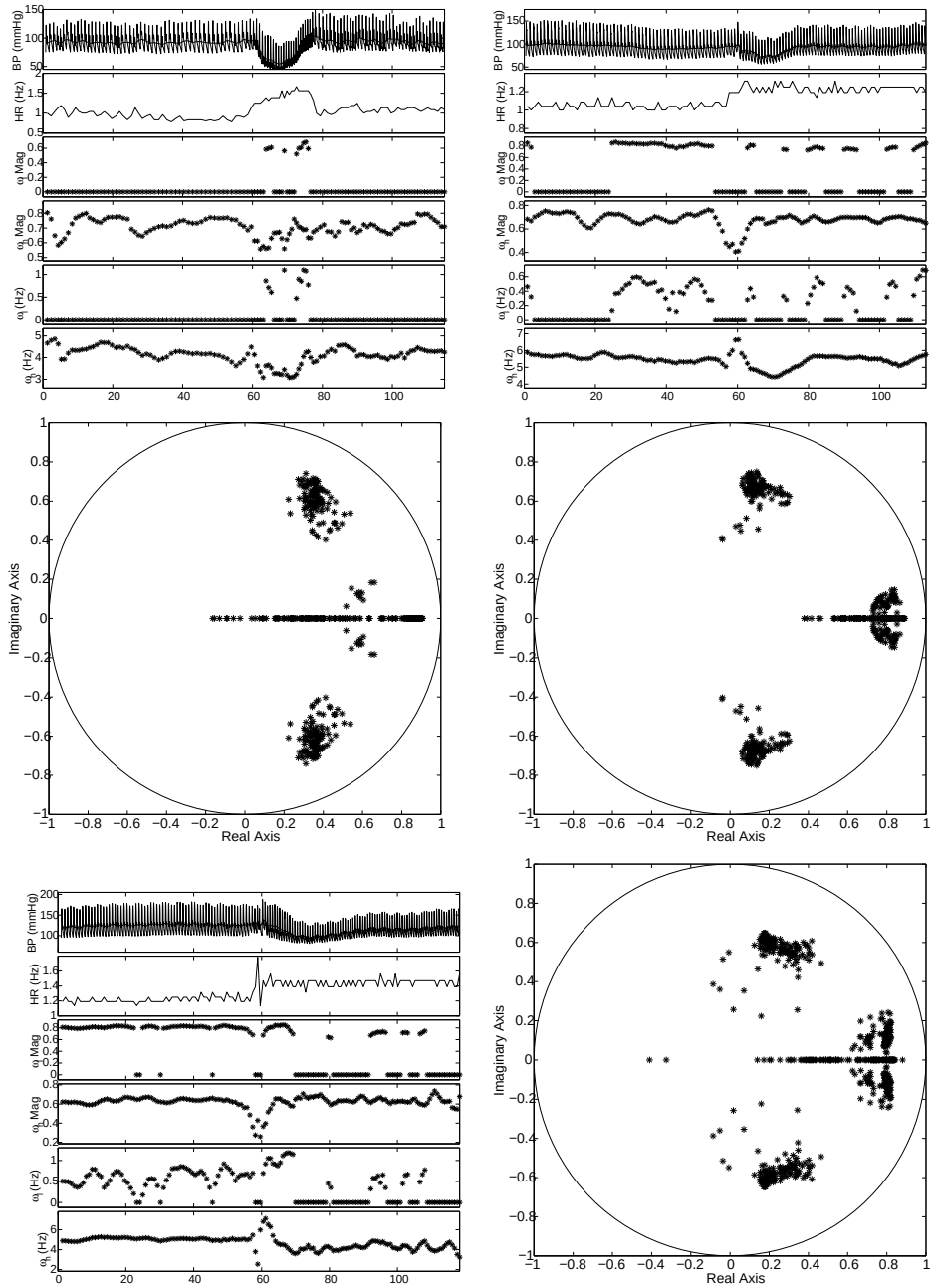

FIGURE 8. Time variation of system poles in the blood pressure (BP) signal for a healthy young subject (left), a healthy elderly subject (right), and a hypertensive elderly subject (bottom). The time variation of the signals is shown, along with a scatter plot of the poles in the complex plane. For the low-frequency pole ω_l a zero value indicates that ω_l was not present for that cycle; instead two real poles were computed. A scatter plot of the poles is given in the complex plane. ω_h is shown as the cluster of poles with higher phase, and ω_l as the poles with lower phase. The separation phase is 3 Hz.

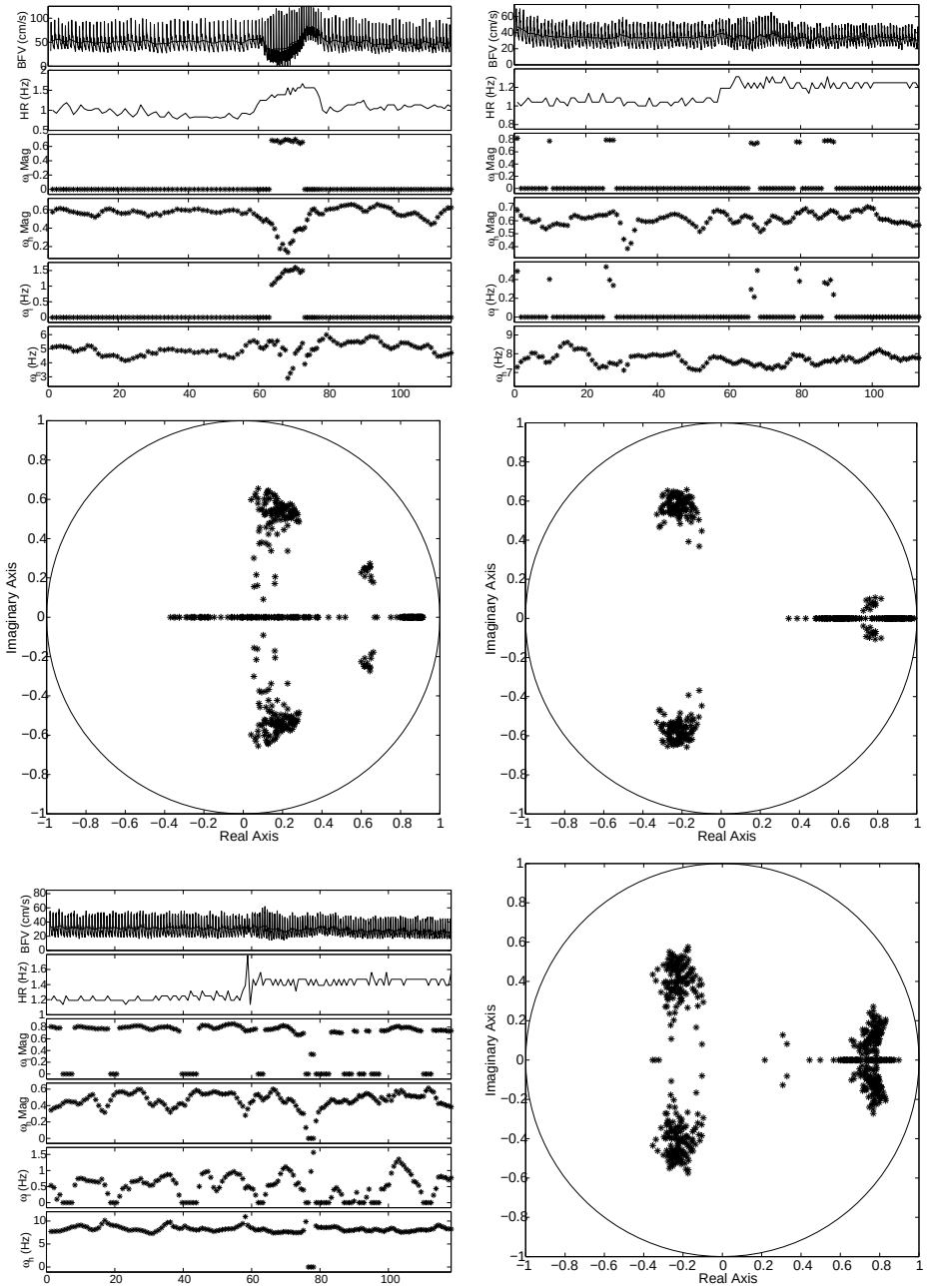

FIGURE 9. Time variation of system poles in the blood flow velocity (BFV) signal for a healthy young subject (left), a healthy elderly subject (right), and a hypertensive elderly subject (bottom). The time variation of the signals is shown, along with a scatter plot of the poles in the complex plane. For the low-frequency pole ω_l a zero value indicates that ω_l was not present for that cycle; instead two real poles were computed. A scatter plot of the poles is given in the complex plane. ω_h is shown as the cluster of poles with higher phase, and ω_l as the poles with lower phase. The separation phase is 3 Hz.

the elderly subjects do not show any significant difference either in magnitude or in frequency. Finally, it is also observed that the ω_h frequency is typically higher for the blood flow velocity signals, than for the corresponding blood pressure signals.

Though not attempted here, interpretations of the changes in these different representations over time might be considered, and analogies may be developed between these results and standard measures such as arterial resistance, compliance, and inertance. If one considers an analog circuit model such as in [20, 31, 32], the system pole magnitudes in Figures 8 and 9 are inversely related to arterial resistance, R, in that a smaller magnitude corresponds to a higher resistance. The pole frequencies, ω, are inversely related to the square root of the compliance, C, inertance, L, product, $\omega = 1/\sqrt{LC}$. Thus a higher pole frequency would imply a lower compliance-inertance product.

It is noted that the tube radii associated with the healthy young subjects show a distinct dilation during the change in posture. It was conjectured that this reflected the greater elasticity of the blood vessels in the healthy young subjects. The pole patterns indicate that the healthy young subjects have a vascular system that damps the impulses more quickly than the older subjects. This is evident from the lower magnitude of the high-frequency poles and the very few cases of low-frequency poles of the healthy young subjects compared to those of the older ones. It is conjectured that the greater elasticity of vessels in younger people results in a system model that shows significantly more damping of the oscillations or no oscillations, as indicated by two real poles.

It is also possible to generate continuous-time models from the discrete-time models computed here. There are several techniques for doing this [42]. The basis for this transformation is the design of digital filters from analog specifications. It should be noted that when transforming from a digital system to an analog system, it is the transfer function that is of interest. There is no way to derive specific values for the individual value of circuit elements of an equivalent analog system unless the architecture of the circuit is severely restricted. The continuous-time parameters may be used in conjunction with previous vascular models. We are investigating these transformations in parallel research.

5. **Conclusion.**

The multipulse method from DSP has been applied to the analysis of blood pressure and blood flow velocity signals measured for subjects undergoing posture change from sitting to standing. The multipulse method assumes that the signals can be generated by passing a series of impulses through an autoregressive filter. The multipulse method computes the location and amplitudes of the impulses along with the AR filter coefficients.

This method has advantages over other approaches used to analyze blood pressure and blood flow velocity signals in that it does not assume any intrinsic coupling between the two. Instead, each signal is the result of some independent input signal (represented here by the pulses) that may come from the heart or the brain. Also, the very accurate signal reconstructions obtained with this method attest to its applicability.

Different time and frequency domain representations of the estimated signal models are presented. These include autoregressive AR filter coefficients, reflection coefficients (calculated but not shown), tube radii, and system poles. These parameters may be related to physical quantities, and the variation of these over

time might prove to give insight into the physiological controls that regulate blood pressure and blood flow velocity during posture change from sitting to standing.

Acknowledgments. This work would not have been possible without the support of and access to data from Dr. Lewis Lipsitz at the Hebrew Senior Life and Harvard Medical School, Boston, MA, and Dr. Vera Novak at the Beth Israel Deaconess Medical Center and Harvard Medical School, Boston, MA. In addition the authors would like to thank the NIH for supporting this work though the grant number R03AG20833 from the NIA Pilot Research Program PA-01-037 and the Faculty and Research Development Fund at North Carolina State University.

REFERENCES

[1] L.A. Lipsitz, S. Mukai, J. Hamner, M. Gagnon, and V. Babikian. Dynamic regulation of middle cerebral artery blood flow velocity in aging and hypertension. Stroke 31(8) (2000) 1897-1903.

[2] B.S. Atal and J.R. Remde. A New Model of LPC Excitation for Producing Natural Sounding Speech at Low Bit Rates. Proc Int Conf Acoust, Speech, Signal Proc 3-5 (1982) 614-617.

[3] A. Parker, S.T. Alexander, and H.J. Trussell. Low Bit Rate Speech Enhancement Using a New Method of Multiple Impulse Excitation. Proc Int Conf Acoust, Speech, Signal Proc 19-21 (1984) 1.5.1-1.5.4.

[4] S.T. Alexander. A Simple Noniterative Speech Excitation Algorithm Using the LPC Residual. IEEE Trans Acust Speech Sign Proc 33 (1985) 432-434.

[5] T.F. Quatieri. Discrete-Time Speech Signal Processing. Prentice Hall PTR, Upper Saddle River, NJ, 2002.

[6] M. Cookey, H.J. Trussell, and I.J. Won. Seismic Deconvolution by Multipulse Methods. IEEE Trans Acust Speech Sign Proc 38 (1990) 156-160.

[7] K. Narayanan, J.J. Collins, J. Hamner, S. Mukai, and L.A. Lipsitz. Predicting Cerebral Blood Flow Response to Orthostatic Stress from Resting Dynamics: Effects of Healthy Aging. Am J Physiol 281(3) (2001) R716-R722.

[8] B.J. Carey, R.B. Panerai, and J.F. Potter. Effect of Aging on Dynamic Cerebral Autoregulation during Head-up Tilt. Stroke 34(8) 2003 1871-1875.

[9] V. Novak, A. Chowdhary, B. Farrar, H. Nagaraja, J. Braun, R. Kanard, P. Novak, and A. Slivka. Altered Cerebral Vasoregulation in Hypertension and Stroke. Neurology 60(2) (2003) 1657-1663.

[10] A. Blaber, R. Bondar, F. Stein, P. Dunphy, P. Moradshahi, M. Kassam, and R. Freeman. Transfer Function Analysis of Cerebral Autoregulation Dynamics in Autonomic Failure Patients. Stroke 28 (1997) 1686-1692.

[11] R.R. Diehl, D. Linden, D. Lucke, and P. Berlit. Spontaneous blood pressure oscillations and cerebral autoregulation. Clin Autonomic Res 8 (1998) 7-12.

[12] R.B. Panerai. Assessment of Cerebral Pressure Autoregulation in Humans–A Review of Measurement Methods. Physiol Meas 19 (1998) 305-338.

[13] R. Zhang, J. Zuckerman, and B. Levine. Deterioration of Cerebral Autoregulation during Orthostatic stress: Insights from the Frequency Domain. J Appl Physiol 85 (1998) 1113-1122.

[14] R. Zhang, J. Zuckerman, C. Giller, and B. Levine. Transfer Function Analysis of Dynamic Cerebral Autoregulation in Humans. Am J Physiol 274 (1998) H233-H241.

[15] R.B. Panerai, S.L. Dawson, and J.F. Potter. Linear and nonlinear analysis of human dynamic cerebral autoregulation. Am J Physiol 277 (1999) H1089-H1099.

[16] R.B. Panerai, S. Dawson, P. Eames, and J. Potter. Cerebral Blood Flow Velocity Response to Induced and Spontaneous sudden changes in Arterial Blood Pressure. Am J Physiol 280 (2001) H2162-H2174.

[17] N. Krishnamurthi, J. Collins, J. Hamner, S. Mukai, and L. Lipsitz. Predicting Cerebral Blood Flow Response to Orthostatic Stress from Resting Dynamics: Effects of Healthy Aging. Am J Physiol 281 (2001) R000-R000.

[18] C.-C. Chiu and S.-J. Yeh. Assessment of Cerebral Autoregulation using Time-Domain Cross-Correlation Analysis. Comp Biol Med 31 (2001) 471-480.

[19] R.B. Panerai, V. Hudson, L. Fan, P. Mahony, P.M. Yeoman, T. Hope, and D.H. Evans. Assessment of dynamic cerebral autoregulation baseed on spontaneous fluctuations in arterial blood pressure and intracranial pressure. Physiol Meas 28 (2002) 59-72.
[20] M. Olufsen, A. Nadim, and L. Lipsitz. Dynamics of Cerebral Blood Flow Regulation Explained Using a Lumped Parameter Model. Am J Physiol 282 (2002) R611-R622.
[21] J.E. Penelope, M.J. Blake, R.B. Panerai, and J.F. Potter. Cerebral Autoregulation Indices are Unimpaired by Hypertension in Middle Aged and Older Individuals. Am J Hypertens 16(9 Pt. 1) (2003) 746-753.
[22] H.R. Warner. The Frequency-dependent Nature of Blood Pressure Regulation by Carotid Sinus Studied with an Electric Analog. Circ Res VI (1958) 35-40.
[23] R.W. DeBoer, J.M. Karemaker, and J. Strackee. Hemodynamic Fluctuations and Baroreflex Sensitivity in Humans: A Beat-to-beat Model. Am J Physiol 253 (1987) 680-689.
[24] F.M. Melchior, R.S. Scrinivasen, and J.B. Charles. Matemathical modeling of the human response to LBNP. Physiologist 35 (Suppl1) (1992) S204-S20.
[25] J.T. Ottesen. Modeling of the baroreflex-feedback mechamism with time-delay. J Math Biol 36 (1997) 41-63.
[26] J.T. Ottesen. Nonlinearity of baroreceptor nerves. Surv Math Ind. 7 (1997) 187-201.
[27] M. Ursino. Interaction Between Carotid Baroregulation and the Pulsating Heart: A Mathematical Model. Am J Physiol 44 (1998) H1733-H1747.
[28] R. Zhang, K. Behbehani, C. Crandall, J. Zuckerman, and B. Levine. Dynamic Regulation of Heart Rate during Acute Hypotension: New Insight into Baroreflex Function. Am J Physiol 280 (2001) H407-H419.
[29] R.D. Lipman, P. Grossman, S.E. Bridges, J.W. Hamner, and J.A. Taylor. Mental Stress Response, Arterial Stiffness, and Baroreflex Sensitivity in Healthy Aging. J Gerontol A Biol Sci Med Sci 57(7) (2002) B279-B284.
[30] R.D. Lipman and J.A. Taylor. Spontaneous Indicies are Inconsistent with Arterial Baroreflex Gain. Hypertension 42(4) (2003) 481-487.
[31] O. Frank. Die Grundform des Arterielen Pulses erste Abhandlung: Mathematische Analyse. Z Biol 37 (1899) 483-526.
[32] N. Stergiopulos, J. Meister, and N. Westerhof. Simple and Accurate Way for Estimating Total and Segmental Arterial Compliance: The Pulse Pressure Method. Ann Biomed Eng 22 (1994) 392-397.
[33] R.B. Panerai, M. Chacon, R. Pereira, and D.H. Evans. Neural Network Modeling of Dynamic Cerebral Autoregulation: Assessment and Comparison with Established Methods. Med Eng Phys 26 (2004) 43-52.
[34] M.S. Olufsen, H.T. Tran, and J.T. Ottesen. Modeling Cerebral Blood Flow during Posture change from Sitting to Standing. J Cardiovasc Eng 4(1) (2004) 47-58.
[35] R. Mukkamala and R.J. Cohen. A Forward Model-Based Validation of Cardiovascular System Identification. Am J Physiol 281 (2001), H2714-H2730.
[36] T. Heldt, E.B. Shim, R.D. Kamm, and R.D. Mark. Computational Modeling of Cardiovascular Response to Orthostatic Stress. J Appl Physiol 92 (2002) 1239-1254.
[37] N. Aljuri and R.J. Cohen. Theoretical Considerations in the Dynamic Closed-Loop Baroreflex and Autoregulatory Control of Total Peripheral Resistance. Am J Physiol 287 (2004) H2252-H2273.
[38] M. Fernandez, V. Milisic, and A. Quateroni. Analysis of a Geometrical Multiscale Blood Flow Model based on the Coupling of ODE's and Hyperbolic PDE's. Multiscale Model Simul 1 (2003) 173-195.
[39] Z.M. Kadas, W.D. Lakin, J. Yu, and P.L. Penar. A Mathematical Model of the Intracranial System Including Autoregulation. Neurol Res 19 (1997) 441-450.
[40] R. Aaslid, K.F. Lindegaard, W. Sorteberg, and H. Nornes. Cerebral autoregulation dynamics in humans. Stroke 20 (1989), 45-52.
[41] A.V. Oppenheim and R. W. Schafer. Discrete-time Signal Processing. Prentice Hall, Englewood Cliffs, NJ, 1998.
[42] J.G. Proakis and D.G. Manolakis. Digital Signal Processing: Principles, Algorithms, and Applications. Prentice Hall, Upper Saddle River, NJ, 1996.

Received on January 17, 2006. Revised on January 30, 2006.

E-mail address: justice@umich.edu
E-mail address: hjt@eos.ncsu.edu
E-mail address: msolufse@math.ncsu.edu